FAZ Publishing
JCF

Journal of Complex Flow, Vol. 2 No. 2 (2020) p. 13-18

Journal of Complex Flow

Journal homepage : www.fazpublishing.com/jcf

e-ISSN : 2672-7374

Numerical Study of Jet Impingement Cooling on a Smooth on 3-D Convex Surface

Wan Nur Aina Nabilah Mohd Zaki[1], Suzairin Md Seri[2,*]

[1]Faculty of Mechanical and Manufacturing Engineering,
Universiti Tun Hussein Onn Malaysia, Batu Pahat, 86400, MALAYSIA

[2] Centre for Energy and Industrial Environment Studies (CEIES),
Faculty of Mechanical and Manufacturing Engineering, Universiti Tun Hussein Onn Malaysia, 86400 Parit Raja, Batu Pahat, Johor Darul Takzim, MALAYSIA

*Corresponding Author

Email: suzairin@uthm.edu.my

Received 12 May 2020;
Accepted 23 August 2020;
Available online 15 October 2020

Abstract: Jet impingement cooling is an alternative method to force a fluid flowing to a target surface in order to remove heat from it. Many applications are implementing this system such as electronic device coolers and cooler for turbine blades. The significance of this application is it can increase the rate of heat transfer towards the fluid. A set of simulations was run in ANSYS Fluent on 2D axis-symmetry of round nozzle tip with a convex target surface. After validation, it was found that the best viscous model that can be used throughout the simulation was a standard *k*-epsilon model. Reynold number, nozzle tip to target surface distance, *L/d*, and target surface radius, *r/d* are the parameters considered. The ranges of the parameters are $5000 \leq Re \leq 100000$, $1 \leq L/d \leq 10$, and $8.86 \leq r/d \leq 20$. The numerical results were validated against the experimental data. The ACFD method was applied to derive an equation that correlates the average Nusselt number to the parameters. The validity of the equation is tested by comparing the output to that of the numerical results. The normalized root means square error percentage, NRMSE %, is 4.91%.

Keywords: Jet impingement cooling, 2D-axisymmetric numerical simulation, thermal performance

1. Introduction

Jet impingement is an invention that is efficient in transferring heat between a surface and a driven fluid. The fluid is forcibly impinged to the surface of the product by directing it through the tip of the jet at high pressure. Effective heat transfer will be obtained between the jet's nozzle and the product's surface [1,2]. Nowadays, this improvement method has been used broadly for various industries. This is because the study shows that the impingement jet is a smart mechanism since it is proficient in achieving the highest rate of heat transfer. It was developed in order to cool a high temperature component or surface by removing a large quantity of heat [3]. The system of this jet cooling impingement is basically made to strike the target surface with a fluid that is high in velocity. It will deliver the most effective and flexible technique in transferring energy and mass for the industrial applications.

A large amount of thermal energy and mass between the geometry's wall and fluid will be transferred effectively since a directed fluid flow is impinged against the surface of the product. Due to these advantages, there is a lot of industries that choose to use the jet impingement cooling system nowadays. The various applications that are widely used are the cooler of stock material, the electronic component's cooler, cooler for a gas turbine blades and metal's annealing [4,5].

The researchers had obtained the empirical correlations in evaluating the local heat transfer together with the average heat transfer of the system. This correlation was expected to be resulted as the development of the flow and thermal boundary layer. In many studies of the heat transfer system, the results showed that the researchers only covered the dimensionless distance of nozzles' diameters from the stagnation point or area [6]. Hence, another two parameters and the shape of target surface are needed to be studied deeply in order to improve the performance of the system.

**Corresponding author: suzairin@uthm.edu.my*

This study aims to investigate the characteristics of thermal and flow field on convex surface caused by jet impingement and to obtain a correlation between flow geometries and the thermal and overall performance of jet impingement cooling by using ANSYS software.

2. Modelling and Methodology

A 2-D axis-symmetry round nozzle with a convex target surface was drawn in the SolidWorks and later it was imported to the ANSYS Fluent R3 Student Version. The dimensions and related parameters were obtained from the previous experiment that was investigated by Lee *et al*. [7]. The validation between experimental result and simulation was done after performing a grid independence test. Another comparison between simulation results and the ACFD correlations was done in order to identify the validation of the new equations of correlation between parameters that will be implemented for future study.

2.1 Governing equations

Based on the scope of this study, the geometry was in a 2-D but axis-symmetry geometry. Hence, the directions of the velocities were classified into three directions which are x, y and z direction. The fluid flow was set to be incompressible and steady flow. So, the continuity equation is given by;

$$\frac{\delta u}{\delta x}+\frac{\delta v}{\delta y}+\frac{\delta w}{\delta z}=0 \tag{1}$$

ACFD is totally about the linear form that is derived from the graph of the correlations. Hence, an equation in a form of y = mx + c is aimed to meet the requirements in deriving a new equation of the relationship between the manipulated variables [8]. Therefore, Taylor Series is applied in order to build the equation.

$$\begin{aligned} Nu_{Ave} = Nu_{AveRef} &+\left(\phi_1-\phi_{1,Ref}\right)\left(\delta Nu_{Ave}/\delta\phi_1\right) \\ &+\left(\phi_2-\phi_{2,Ref}\right)\left(\delta Nu_{Ave}/\delta\phi_2\right) \\ &+\left(\phi_3-\phi_{3,Ref}\right)\left(\delta Nu_{Ave}/\delta\phi_2\right) \end{aligned} \tag{2}$$

The average Nusselt number is known as the y-axis while *x*-axis is denoted as $\emptyset_n - \emptyset_{nRef}$. Equation 3 shows the formula of the gradient that is used in the Equation 2.

$$m=\frac{\delta Nu_{Ave}}{\delta\theta_n} \tag{3}$$

In order to identify whether this ACFD method is valid or not, a normalized root mean square error (NRMSE) is performed by applying the formula given in the Equation 4.

$$NRMSE=\frac{RMSE}{y_{1,\max}-y_{1,\min}}\times 100\% \tag{4}$$

where the root mean square is given by;

$$RMSE=\sqrt{\frac{\sum_{r=1}^{n}\left(y_1-y_2\right)^2}{n}} \tag{5}$$

2.2 Geometry modelling

The geometry was drawn in SolidWorks 2018 on a *x*-*y* plane since it was in a 2-D axis-symmetry. Fig. 1 shows the overall domain of the jet impingement and its dimensions. The unit was set in centimeter since the original one was in that unit. To avoid any miscalculation in converting the unit, the non-SI unit was used for the drawing in the SolidWorks.

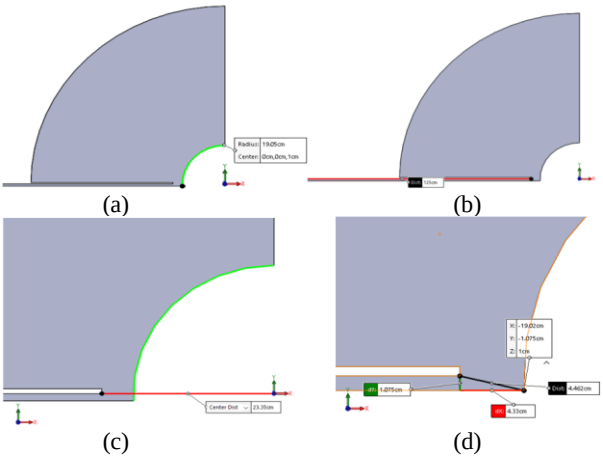

Fig. 1 - Dimensions and close-up view of jet impingement cooling's geometry: (a) Radius of curvature; (b) Length of nozzle; (c) Distance nozzle's tip to target surface; (d) Diameter of nozzle

2.3 Meshing

There are three types of modifications that were being implemented in this meshing process, excluding the default meshing which are face sizing, inflation and all triangles method [9, 10]. First modification was inflation after the generating the default meshing. Later, the triangle method was implemented for the modification meshing. The full view and close-up view of final meshing are shown in Fig. 2 and Fig. 3

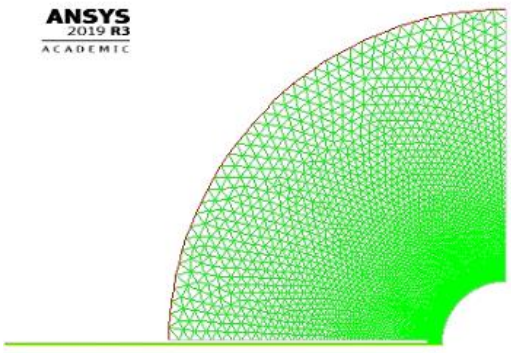

Fig. 2 - Final meshing

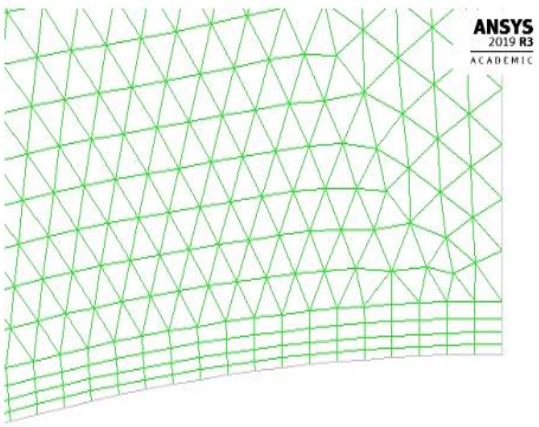

Fig. 3 - Close up view

2.4 Boundary condition

Boundary condition was first set up before doing the meshing by naming the boundary first. Then, the magnitude for each boundary will be inserted at the Fluent's Setup before running the calculation. Table 1 shows the summary of the boundary conditions and Fig. 4 shows it named selection in meshing.

Table 1 - Boundary conditions and values

Label	Boundary condition	Value
A	Velocity Inlet	7.47 m/s
A	Temperature Inlet	300 K
B	Pressure Outlet	0 Pa
B	Temperature Outlet	300 K
C	Wall Temperature	500 K

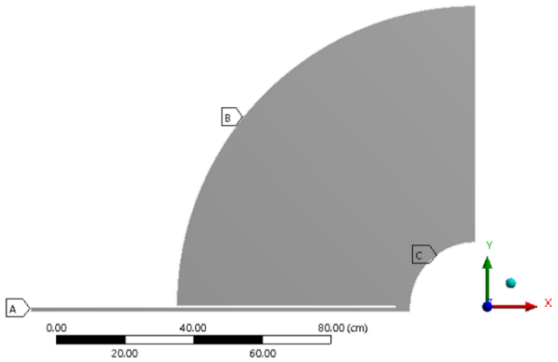

Fig. 4 - Label of named selection for boundary condition

2.5 Grid independence test

In order to determine the best method for meshing process, a changing in growth rate is set by incrementing the value of the element size. There are six continuous tests that have been done regarding the trend in growth rate which the trend is starting with a growth rate of 1.02 and wrapping the it up with 1.08 of growth rate. From the validation, geometry with Reynolds number, *Re* = 11000 and the *L/d* = 2 is used for the grid independence test. Since the growth rate is increasing in magnitude, the number of elements is decreasing due to the increment in size [11-13].

The number of nodes also decreases since the element decrements in number too. Fig. 5 shows the result of the grid independence test that was plotted in a graph of Nusselt number against the r/d. Table 2 shows the relative errors that was corresponding to the growth rate. The growth rate of 1.07 was chosen as the best meshing method because it has neither the highest nor the lowest relative error.

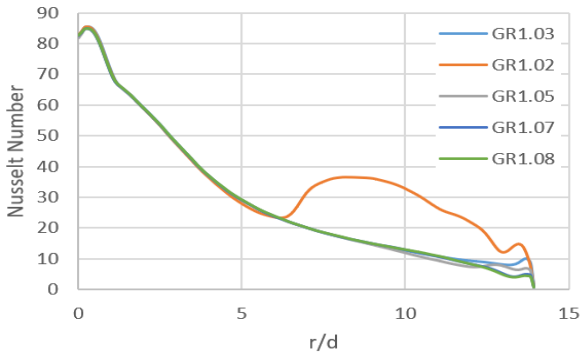

(a)

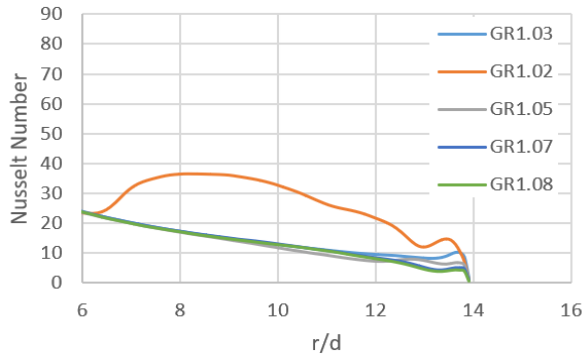

(b)

Fig. 5 - Grid independence test: (a) Full graph of average Nusselt number vs r/d; (b) Graph of average Nusselt number vs r/d for $6 \leq r/d \leq 14$.

Table 2 - Relative errors that was corresponding to the growth rate

Number of Nodes	Number of Elements	Average Nusselt Number	Relative Error
18930	35841	36.75	-
11734	21539	29.47	19.8 %
7126	12399	28.87	2.03 %
5373	8929	28.99	0.41 %
4898	7989	28.91	0.3 %

3. Results and Discussion

The pressure contour and velocity vector are discussed based on the data obtained for different value of Reynold number. The correlation between those three parameters are plotted to observe the trend of the average Nusselt number due to the manipulated variables. An equation of ACFD correlation was derived from the Taylor Series expansion method.

3.1 Correlation between parameters

Fig. 6 shows that the linear graph of average Nusselt number against Reynold number is directly proportional to each other. For this case, the diameter of 0.0215 m and dimensionless *L/2* equals to 2 was set to be constant while average Nusselt number is depending to the Reynold number. When the Reynold number is increasing, the average Nusselt number will increase too and vice versa. This is proven by the equation of Nusselt number. The highest average Nusselt number is found to be 140 when the Re = 100000 while the lowest average Nusselt number is recorded to be below 40 when the Reynold number of the air is set to be below than 20000.

Based on Fig. 7, the trend of the graph of average Nusselt number against the distance of nozzle to the convex surface, *L/d* is varying at each of the dimensionless value. The dimensionless distance of streamwise from the point of stagnation which is *r/d* and the Reynold number is set as constant with the value of 8.86 and 23000, respectively. For *L/d* that is equal to 1, the average Nusselt number that is resulted from it is 48.54953. Later, when the dimensionless *L/d* is increasing to 2, the value decreases to 47.90643. However, when *L/d* is equal to four, the responding variable is decreasing steadily by 0.25414. The graph is then decreasing abruptly by 0.76111 when the manipulated variable is increasing by 2. However, when *L/d* is equal to 8, the average Nusselt number is increasing rapidly from 47 to 51.25.

Meanwhile, Fig. 8 show the average Nusselt number is depending directly to the dimensionless distance of the streamwise from the stagnation point, r/d while the Reynold number and the *L/d* is a constant where their values are 23000 and 2, respectively. The graph shows a trend where the increment of the average Nusselt numbers are found to be the same for all of them which is 0.4. However, the first increment of them is increasing abruptly since the difference value between the two first two points of *r/d* is below than 5. Meanwhile, the last two lines show that the average Nusselt number is increasing gradually when the manipulated variable is added to 5.

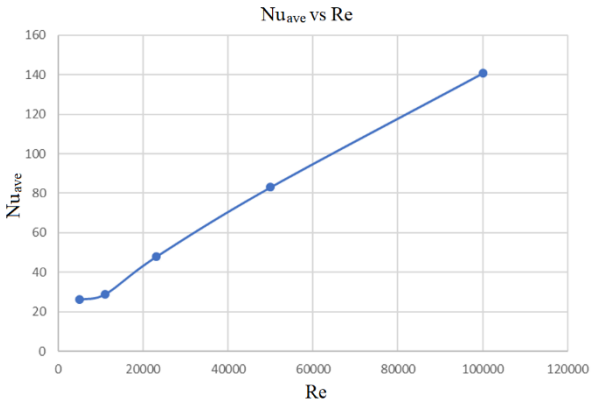

Fig. 6 - Average Nusselt number against Reynold number

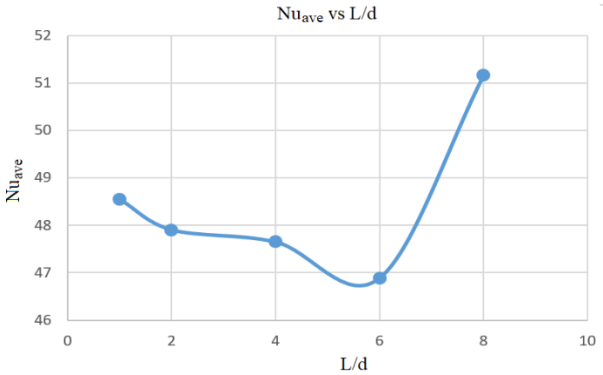

Fig. 7 - Average Nusselt number against the distance of nozzle to the convex surface

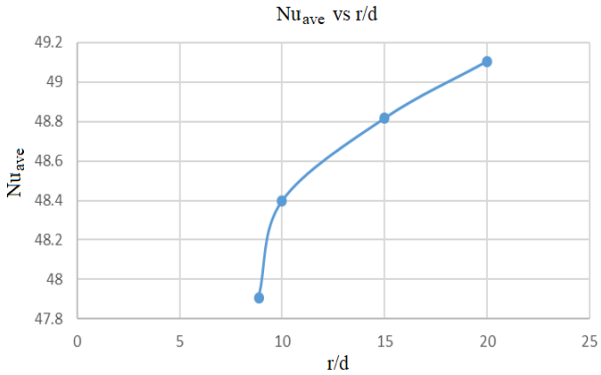

Fig. 8 - Average Nusselt number is depending directly to the dimensionless distance of the streamwise

3.2 Validation between simulation and pervious study

Based on the Fig. 9, the graph of Nusselt number against dimensionless distance of streamwise from the stagnation point is showing two differences kind of trends for all the types of the viscous model. These viscous models are simulated in order to choose the best viscous model that can be applied once the parameters are changing since previous researcher did not mention the suitable model that can be used to validate his experiment and study [5]. In the figure, doted dark blue line is representing the graph that is obtained from the previous paper. Meanwhile, the rest lines are based on the data resulted from the simulation for different models. Four of the lines except the k-epsilon's line are showing the same trend of data where the Nusselt number are increasing rapidly for the first 1.000 of *r/d*. Then, the graph is starting to decrease progressively along the rest 4.000 of the dimensionless distance of *r/d*.

Despite having the difference in the trend of graph, the k-epsilon viscous model's shows that it has the best line that is almost as the experimental one. Instead, the data that is obtained from the k-epsilon's simulation is the most validate one since the percentage of error between the simulation results and experimental values is below than 10% which is 9.5%. The average Nusselt number for the simulation and the experimental result are 55.484 and 61.333, respectively. Hence, below is the calculation of the percentage error for this validation. Since the k-epsilon model is validated to the Lee's result, this type of model is used for all the simulations for different parameters.

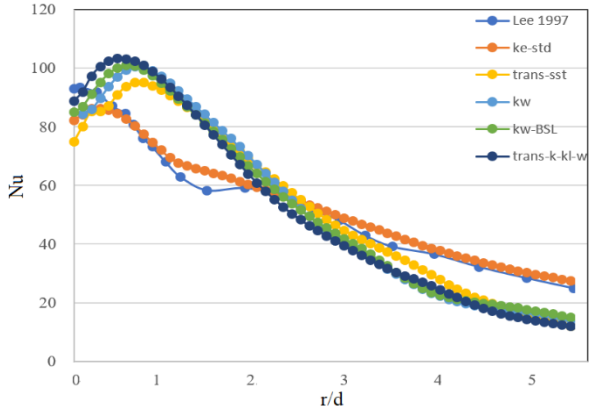

Fig. 9 - Graph of Nusselt number vs. r/d for different types of viscous model

3.3 Linearization

From the correlation shown in Fig. 10, three equations were derived from the graphs. The equations are in term of phi with respect to the related parameters. By substituting the parameters value, the values of phi will be obtained. Hence, graph of linearization will be plotted. Equations 6, 7 and 8 show the derived equation that were resulted from the correlations graph.

$$\phi_1 = 0.0012\mathrm{Re} + 18.355 \tag{6}$$

$$\phi_2 = 0.0232\left(L/d\right)^4 - 0.3488\left(L/d\right)^3 + 1.8012\left(L/d\right)^2 + 3.9533\left(L/d\right) + 51.027 \tag{7}$$

$$\phi_3 = 0.0048\left(r/d\right)^3 - 3.9533\left(r/d\right)^3 + 32.694 \tag{8}$$

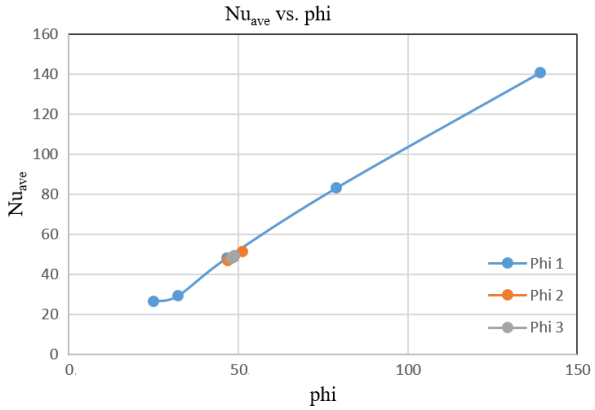

Fig. 10 - Combination graphs of linearization

Fig. 10 also shows the combination graphs of linearization. From the graph and the tabulated data, few reference values of phi can be found from them based on the reference value of average Nusselt number which is 47.906. Table 3 summarizes all the data that will be used to plot the ACFD correlation by listing out the reference value of phi and the gradient obtained from the equation of line.

Table 3 - Summary of ACFD correlation

$\emptyset_{\mathrm{Ref}}$		Corresponding Parameter with its value		$\delta \mathrm{Nu}_{\mathrm{Ave}}/\delta\emptyset = \mathrm{Gradient}, m$
$\emptyset_{1Ref}$	46.56	Re	23000	1.204
$\emptyset_{2Ref}$	47.91	L/d	2	1.008
$\emptyset_{3Ref}$	47.91	r/d	8.86	1.155

3.4 Parity Plot from Taylor Series expansion and NRMSE

The average Nusselt number was calculated by using Equation 2. From this tabulated data obtained, graph of average Nusselt number by simulation versus ACFD's was plotted. Based on the Fig. 11 which represents the Parity plot, the graph is not in the best fit since there is a few data that is not touching the line. Meanwhile, RMSE is the data that was obtained from the calculation in determining the NRMSE. This calculation was applying the Equation 4 and 5. The result of the NRMSE which is 4.91% indicates that the ACFD method and its equations derived from the Taylor Series are valid since the error is below 10%.

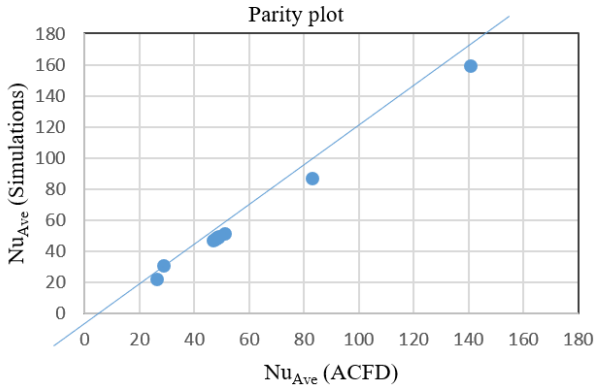

Fig. 11 - Parity plot of average Nusselt number for simulation against ACFD

4. Conclusion

As a conclusion, this current numerical study of average Nusselt number on the convex surface is valid to be used and discussed for future reference since the percentage of error for average Nusselt numbers that were resulted from the simulation were below 10%. Besides, the behavior of the fluid flow is exactly same as those that were stated in most of the research papers. The pressure contour of the air from the nozzle of this jet impingement system is found to be highest at the peak of the target surface. Meanwhile, the velocity contour of this fluid is in zero value once it hits the curved surface due to the stagnation area.

This fluid's behavior is supported by many previous studies that carried out the same study, but the results were observed by undergoing a lot of experiments. Besides, the velocity vector that was observed from this numerical study shows another behavior of the fluid flow due to the difference Reynold numbers that were applied throughout this study. It is found that the smaller the Reynold number,

the bigger the circle of the vortex and the fastest it can be formed due to this manipulated variable. This is because a fluid with a smaller Reynold number tends to be disturbed by any other disturbance when it flows through out a shaped surface. Apart from that, this study succeeds in determining the correlation between the parameters such as the Reynold number, the dimensionless distance of nozzle to target surface and the dimensionless distance of the streamwise to the stagnation area. All the parameters do affect the result of average Nusselt number differently. Therefore, an ACFD method was done to derive the linear equations that are corresponding to the correlation to ease the future study in determining the output by substituting any value from each of the manipulated variables.

This method is validated by applying the NRMSE and the percentage of error that was calculated is 4.91%. Hence, this method and its equation are acceptable and valid to be used for the next study. This study itself should be improvised in order to obtain the most significant result. One should learn on how to gain the previous data that were limited and not complete from the previous paper. A contact with the man who carried out the study should be learned and updated. This study is also suggested to cover other type of fluids so that a new study regarding the behavior of fluid due to the density can be carried out and implement it to the real-life application. This will bring different outcomes and result that is affected by the new applying the linear equation from the derivation of the ACFD.

Acknowledgement

The authors thank to the all industries partner and Universiti Tun Hussein Onn Malaysia (UTHM) for the award of grant and equipment support for the project.

References

[1] Data, R.U.S.A. and Davis, P.E.W. “United States Patent (19) U.S. Patent,” No. 19, 1978.

[2] Gau, C. and Chung, C.M., “Surface curvature effect on slot- air-jet impingement cooling flow and heat transfer process,” *J. Heat Transfer*, 113(4) (1991): 858-864. doi: 10.1115/1.2911214.

[3] Zuckerman, N. and Lior, N., “Jet impingement heat transfer: Physics, correlations, and numerical modeling,” *Adv. Heat Transf.*, 39(C) (2006): 565-631. doi: 10.1016/S0065-2717(06)39006-5.

[4] Jambunathan, K., Lai, E., Moss, M.A. and Button, B.L., “A review of heat transfer data for single circular jet impingement,” *Int. J. Heat Fluid Flow*, 13(2) (1992): 106-115.

[5] R. Gardon and J. C. Akfirat, “Heat Transfer Characteristics of Impinging Two-Dimensional Air Jets”. *J. Heat Transfer*, 88 (1966): 101-107 doi: 10.1115/1.3691449.

[6] Norman, Mohd Azim, and Muhamad Najib Hassan. “Flow Visualization of Perforated Baffles and Impellers for Stirred Tank Reactor with Single Stage Rushton Turbine.” *Journal of Complex Flow* 1 (1) (2019): 21-25.

[7] Lee, D.H., Chung, Y.S. and Kim, D.S., “Turbulent flow and heat transfer measurements on a curved surface with a fully developed round impinging jet,” *Int. J. Heat Fluid Flow*, 18(1) (1997): 160-169.

[8] T. S. O’Donovan and D. B. Murray, “Fluctuating fluid flow and heat transfer of an obliquely impinging air jet,” *Int. J. Heat Mass Transfer*, 51(25-26) (2008): 6169–6179, doi: 10.1016/j.ijheatmasstransfer.2008.04.036

[9] J. M. Bergthorson, K. Sone, T. W. Mattner, P. E. Dimotakis, D. G. Goodwin, and D. I. Meiron, “Impinging laminar jets at moderate Reynolds numbers and separation distances,” *Phys. Rev. E - Stat. Nonlinear, Soft Matter Phys.*, 72(6) (2005): 1–12

[10] A. Abdel-Fattah, F. S. Abou-Taleb, and G. H. Moustafa, “Behavior of air jet impinging on curved surfaces,” *J. Aerosp. Eng.*, 27(5) (2014): 1–11, doi: 10.1061/(ASCE)AS.1943-5525.0000352.

[11] A. S. Fleischer, K. Kramer, and R. J. Goldstein, “Dynamics of the vortex structure of a jet impinging on a convex surface,” *Exp. Therm. Fluid Sci.*, 24(3-4) (2001): 169–175, doi: 10.1016/S0894-1777(01)00051-6.

[12] Manshoor, B., Sapit, A., Nordin, N., Hariri, A., Salleh, H., Razali, M.A., Zaman, I., Khalid, A., Ghazali, M.F., and Alsayed, M.K., “Simulation Of Fractal Like Branching Microchannel Network On Rectangular Heat Sink For Single-Phase Flow”, *CFD Letter*, 1(69) (2020): 69-79

[13] Pramiyanti, Y., Seri, S.M., and Sapit. A. “Incompressible Turbulent Swirling Flow through Circle Grid Perforated Plate”. *Journal of Complex Flow* 2(1) (2020): 11-16